Investigating the Effect of Various Heteroatom Dopants on Reduced Graphene Oxide's (rGO) efficiency in degradation of Organic Pollutants

Jonathan Lee (4i2), Terng Juin Chih (4i2)

01-11

Abstract

Rapid industrialisation over recent years has led to the rampant discharge of organic pollutants such as direct red dye into water bodies. Such dyes pollute the water, posing a threat to those who rely on these drinking sources. Peroxymonosulfate (PMS) has gained attention as a possible remedy due to the production of highly reactive radical species that can oxidise toxic organic compounds into less harmful products upon activation. Heteroatom-doped reduced graphene oxide has emerged as a potential activation method for PMS, but minimal studies have been conducted to compare the effects of various heteroatom-doped reduced graphene. This study compared the degradation potential of sulfur and boron-doped reduced graphene oxide in the degradation of direct red dye, which showed that both heteroatom-doped graphene oxides were equally effective in the activation of PMS and outperformed pristine graphene in the degradation of direct red dye. Both boron-doped reduced graphene oxide (B-rGO) and sulfur-doped reduced graphene oxide (S-rGO) outperformed pristine graphene in the adsorption of direct red dye by close to 8 times, with B-rGO also outperforming S-rGO in the adsorption of direct red dye. S-rGO and B-rGO both equally outperformed pristine graphene in terms of amount of OH• produced from the activation of PMS, thereby showing that both S-rGO and B-rGO have great potential to be used to degrade toxic organic compounds in wastewaters.

1. Introduction

Rapid industrialisation over the past couple of years has led to water pollution becoming a pertinent issue. Untreated wastes from industries are frequently discharged directly into the environment, causing adverse impacts on both the environment and human (Mayor, 2017).

Common pollutants found in wastewaters includes organic dyes. Organic dyes are commonly used in the textile industry, with 1.3 million tons of dyes and pigments produced and used by the textile industry annually. However, due to inefficient dyeing processes, 2-20% of these dyes and pigments are often discharged as untreated aqueous effluent into water bodies, leading to severe water pollution (Mia et al., 2019). For example, in Jajmau, India, both river and ground water are unfit for drinking, irrigation and general consumption due to dye pollution (Beg & Ali, 2008). One common example of dyes is direct red dye, which is a toxic azo-based

dye used in the textile industry that can cause major health effects which include carcinogenic and mutagenic effects (Novotny et al., 2006).

Peroxymonsulfate (PMS, HSO_5^-) has recently attracted much attention as a potential remedy to water pollution. PMS is a strong oxidizer, with the redox potential of +1.82V. However, PMS has a low reaction rate when reacted directly with organic pollutants such as direct red dye. As such, to effectively degrade organic pollutants, PMS has to be activated to form two strong oxidizer, hydroxyl radicals ($OH\bullet$) and sulfate radicals ($SO_4^{-}\bullet$). Both radical species are strong oxidants, with a redox potential of +2.8V and +2.5V respectively. As such, they have the ability to destruct the structure of organic compounds, breaking them down to less toxic substances (Wang & Wang, 2018).

Many activation methods have been proposed for the activation of PMS, such as heat activation and alkaline activation. However, they each carry their own disadvantages. For example, for heat activation, PMS has to be heated at high temperature to activate it through the fission of O-O bond in the structure of PMS, which has a bond energy ranging from 140-213.3 kJ mol^{-1}. Such an energy intensive process makes heat activation expensive for large scale water purification. Alkaline activation is another alternative, with the main mechanism being the nucleophilic attack on the O-O bond on PMS. However, after degradation, the treated water has to be readjusted to a neutral pH in order to ensure the water is safe for consumption, thus complicating the water purification process (Wang & Wang, 2018).

Reduced graphene oxide (rGO) has received a great deal of attention as a good catalyst for PMS due to its relative huge surface area, high pore volume and its reusability (Devi, Das & Dalai, 2016). It is postulated that the sp^2 hybridized covalent carbon network and oxygen functional groups at the defective edges of the carbon network conducted a redox cycle for electron transfer to PMS to produce hydroxyl radicals and sulfate radicals.

rGO can be heteroatom-doped to increase its catalytic ability. Heteroatom doping can be categorized into 2 types, negative-doping and positive-doping. Negative-doping occurs when rGO is doped with a heteroatom with more valence electrons than C, such as sulfur-doping. Positive-doping occurs when rGO is doped with a heteroatom with lesser valence electrons than carbon, such as boron-doping.

However, minimal studies have been conducted that directly compared each heteroatoms' ability to increase the catalytic ability of rGO for the activation of PMS. Additionally, sulfur-doped graphene has never been applied for PMS activation.

Objectives and Hypothesis

This study aims to synthesize heteroatom (B, S) doped rGO through a reaction between graphite oxide and heteroatom precursor. The catalytical ability of each heteroatom-doped rGO on the activation of PMS was evaluated on the degradation of direct red dye and relative concentration of OH• produced after the activation of PMS.

This study hypothesizes that heteroatom-doped rGO can be synthesized through a reaction between graphene and heteroatom precursor, with both heteroatom-doped rGO being more effective than pristine graphene in the adsorption and degradation of direct red dye. It is also hypothesized that both heteroatom-doped graphene oxide would also have a higher relative concentration of OH• than pristine graphene.

2. Materials and Methods

2.1 Materials

$KMnO_4$, NaOH, H_2O_2, Na_2S and ethanol were procured from GCE Chemicals, concentrated H_2SO_4 and 5% HCl were purchased from Scharlau. Direct red dye, ammonium pentaborate octahydrate, PMS, terephthalic acid and graphite oxide were purchased from Sigma Aldrich.

2.2 Methods

2.2.1 Synthesis of graphite oxide

3.0g of graphite powder was added to 50cm^3 of concentrated H_2SO_4 under stirring in an ice bath. $KMnO_4$ (6.0 g) was added slowly to keep the temperature of the suspension lower than 20 °C. Subsequently, the solution was heated at 35 °C and stirred for 2h. Next, 150 cm^3 of DI water was added, before being stirred for 30 min at 90 °C. 10cm^3 of H_2O_2 was then added slowly to reduce the residual $KMnO_4$ to soluble $MnSO_4$ in an acidic medium, as seen in the following equation:

$$2KMnO_4\,(s) + 5H_2O_2\,(aq) + 3H_2SO_4\,(aq) \rightarrow 2MnSO_4\,(aq) + K_2SO_4\,(aq) + 8H_2O\,(l) + 5O_2\,(g) \quad ---(1)$$

The mixture was filtered and washed with 85cm^3 of HCl to remove the remaining metal sulfates, before being washed with DI water until pH neutral and dried until constant mass.

2.2.2 Synthesis of pristine graphene

10mg of graphite oxide was dispersed in 10cm^3 of water and sonicated for 2h to form single layers of graphene oxide. This solution was then mixed with 10cm^3 of water, before

being refluxed at 100°C for 24h. The precipitate was then washed with water and ethanol before being dried to constant mass.

2.2.3 Synthesis of boron-doped rGO

20mg of graphite oxide was dispersed in 1cm^3 of ethanol and sonicated for 30 min. 20mg of ammonium pentaborate octahydrate was then added to the dispersion before the being refluxed at 60°C for 1h. The mixture was then filtered and the solid retrieved was washed with DI water. The solid was dried until constant mass before being calcined at 350°C for 1h.

2.2.4 Synthesis of sulfur-doped rGO

3mg of graphite oxide was dispersed in 5cm^3 of DI water, before being sonicated for 30 min to form a homogenous graphene oxide suspension. 1cm^3 of 0.5 mol dm^{-3} Na_2S solution was then added to the suspension, before being sonicated at 70°C for 2h. The solid was then retrieved and washed with DI water before being dried until constant mass.

2.2.3 Characterisation of heteroatom-doped rGO

The heteroatom-doped rGO samples synthesised were characterised using Fourier-Transform Infrared Spectrometer (FTIR), Energy Dispersive X-Ray Spectroscopy (EDX) and Scanning Electron Microscope (SEM).

2.2.4 Degradation studies

2.2.4.1 Calibration curve for direct red dye

Calibration curve of direct red dye was prepared by diluting 50 ppm of stock dye to solutions of varying concentrations. The absorbance of each concentration was measured at wavelength 526.5 nm with a UV-VIS spectrophotometer (Shimadzu UV 1800). Graphs of absorbance against concentration were plotted. The calibration curves (Appendix A, pg13) were used to determine the concentration of each dye in all subsequent experiments.

2.2.4.2 Degradation of direct red dye

0.1g of heteroatom-doped rGO was added to 25cm^3 of solution containing 50mg/L of pollutant and 0.5g of PMS in a beaker and stirred for 30min. A control containing the same volume and concentration of pollutant but without any heteroatom-doped rGO was included. 5 replicates were conducted for each type of rGO. The mixture was then centrifuged, with the absorbance of the supernatant measured using a UV-Visible Spectrophotometer (Shimadzu UV-1800) for direct red dye. The percentage of dye removed was calculated using the following formula:

$$Percentage\ removed = \frac{Initial\ concentration - Final\ concentration}{Initial\ concentration} \times 100\%$$

2.4 Analysis of generation of hydroxyl radicals by heteroatom-doped rGO

Heteroatom-doped rGO and PMS were added to 20cm^3 of a mixture of 0.2mmol dm^{-3} terephthalic acid and 1.4mmol dm^{-3} sodium hydroxide and stirred for 15 minutes. After which, the photoluminescence of the resulting solution was measured using a spectrofluorometer. Details of how the concentration of OH• is quantified can be found in appendix B.

3. Results and Discussion

3.1 Characterisation of heteroatom-doped rGO

3.1.1 By Fourier Transform Infrared Spectroscopy (FTIR)

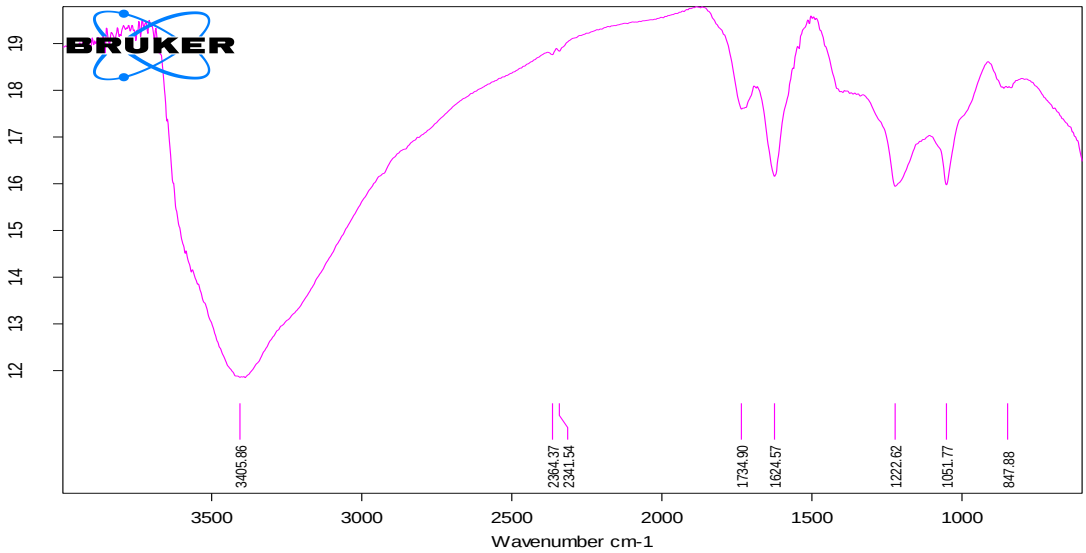

Figure 1(a): FTIR spectra for S-rGO

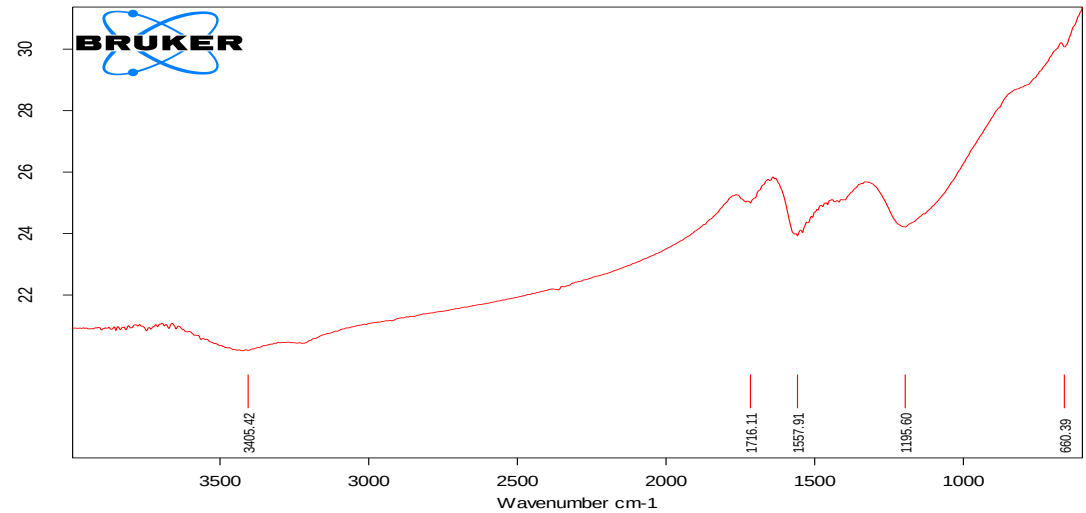

Figure 1(b): FTIR spectra for B-rGO

The FTIR spectra of S-rGO (Figure 1(a)) and B-rGO (Figure 1(b)) both reveals peaks corresponding to O-H stretching (3406cm^{-1}), C=O stretching (around 1735cm^{-1}), C-OH stretching vibration (around 1223cm^{-1}), which are characteristics of rGO. When compared to

the FTIR spectra of pristine graphene (Appendix C, pg16), the relative intensities of O-H, C=O and C-OH bonds were reduced, which is due to an increase in the degree of sp^2 domains and annellation of surface O-H group in S-rGO and B-rGO. For B-rGO, an additional peak corresponding to C-B stretching (1,196 cm^{-1}) was visible. Both spectra are in agreement with those reported in literature (Duan, Indrawirawan, Sun & Wang, n.d.; Karikalan et al., 2017).

3.1.2 By Energy Dispersive X-Ray Spectroscopy (EDX)

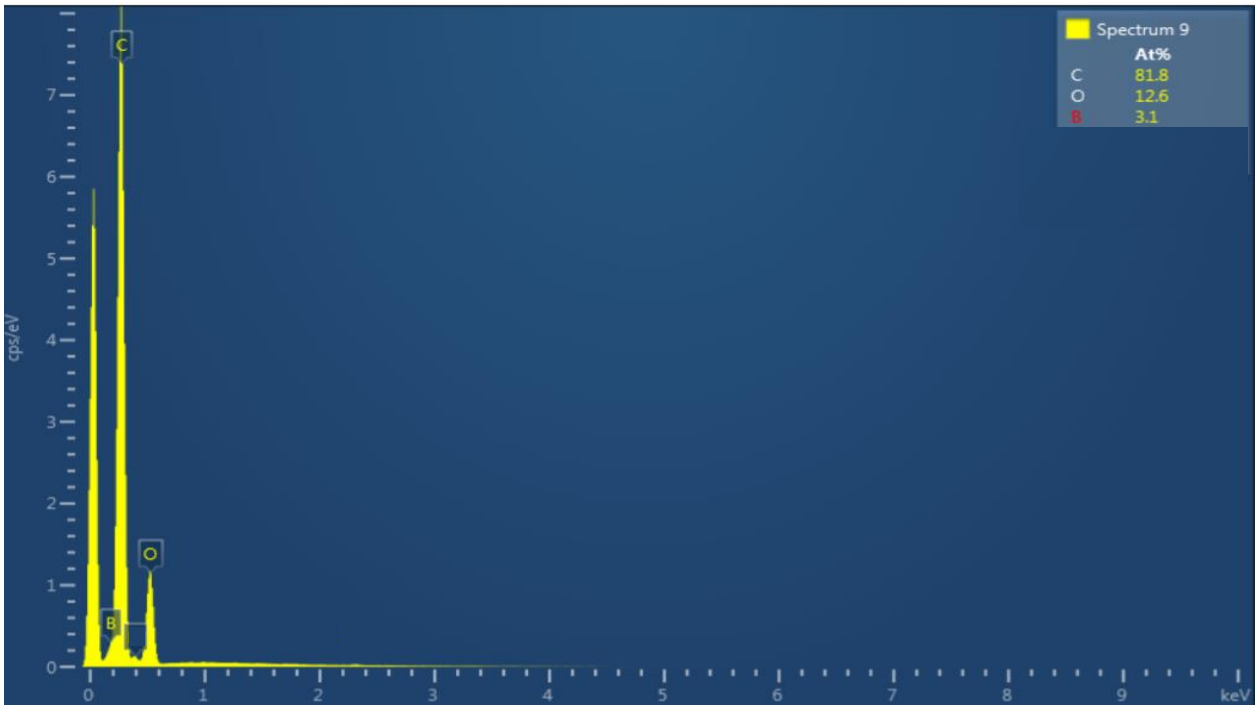

Figure 2: EDS spectrum for B-rGO

Figure 2 shows peaks indicating the presence of boron, oxygen and carbon, showing that B-rGO has been successfully synthesised. EDX analysis could not be conducted for S-rGO due to constraints imposed by the COVID-19 pandemic.

3.1.3 By Scanning Electron Microscope (SEM)

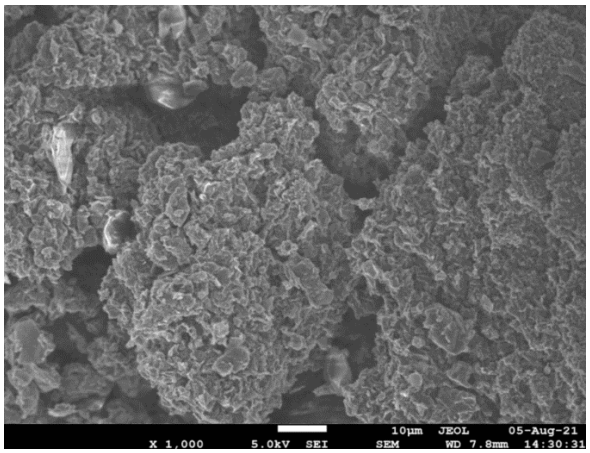

Figure 3: SEM imaging for B-rGO

Figure 3 shows that B-rGO synthesised is rough and uneven. SEM imaging unfortunately could not be conducted for S-rGO due to the constraints imposed by the COVID-19 pandemic.

3.2 Effect of PMS on removal of direct red dye

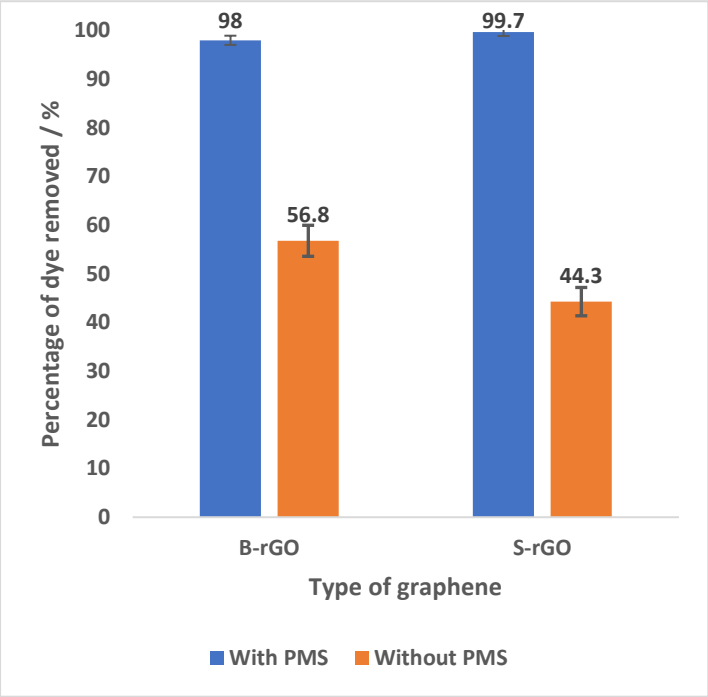

Figure 4: Effect of PMS on removal of direct red dye

Figure 4 shows that there both heteroatom-doped rGOs are more effective in the degradation of direct red dye in the presence of PMS, thereby confirming that both rGOs are effective in the activation of PMS.

Without PMS, both heteroatom-doped rGOs and pristine graphene are able to adsorb both dyes through the formation of π-π interactions between the dye's aromatic backbone and the hexagonal skeleton of both rGOs and pristine graphene.

In the presence of PMS, $SO_4^{-}\bullet$ and OH• will be generated by the activation of PMS by both heteroatom-doped rGO and pristine graphene and start attacking the dye molecule. Defective sites and edges present at the boundary of rGO and pristine graphene can generate dangling σ bonds with unconfined π-electron environment. These edging sites and defective sites, with a closer Fermi level to the bulk structure, unpaired π electrons, and localised spins along the boundaries, are reported to perform as radical-like sites which are able to initialize a radical pathway and facilitate PMS to be converted to $SO_4^{-}\bullet$ and by OH• via charge transfer (Duan et al., 2016). The redox reactions are as follows:

$$C\text{-}\pi^{+} + HSO_5^{-} \rightarrow C\text{-}\pi + OH^{-} + SO_4^{-}\bullet \quad \text{--(2)}$$

$$SO_4^{-}\bullet + H_2O \rightarrow OH\bullet + HSO_4^{-} \quad \text{--(3)}$$

$$SO_4^{-}\bullet + OH\bullet + \text{organic molecules} \rightarrow CO_2 + H2O + \text{residue} \quad \text{--(4)}$$

Equation (2) would represent the possible redox reaction occurring at the defective sites and edges of rGO and pristine graphene (C-π^{+} edge), where PMS is oxidised into $SO_4^{-}\bullet$. Equation (3) would represent the conversion of $SO_4^{-}\bullet$ to OH•, before both radicals attack the organic dye as seen in equation (4). It is postulated that both radical species are able to

simultaneously degrade organic compounds, such as direct red dye, through mechanisms such as desulfonation and hydrogen abstraction.

As such, in the presence of PMS, the overall degradation reaction would involve both the adsorption of the dye molecule and the degradation of the dye molecules. Direct red dye molecules are firstly adsorbed onto the surface of the rGOs or pristine graphene, thereby saturating the surface of the rGOs or pristine graphene and making it easier for the radical species to attack the dye molecule. PMS is being oxidised by rGOs to form $SO_4^{-}\bullet$ and OH•, which will then start attacking and degrading the dye molecule.

3.3 Effect of heteroatom doping on removal of direct red dye without PMS

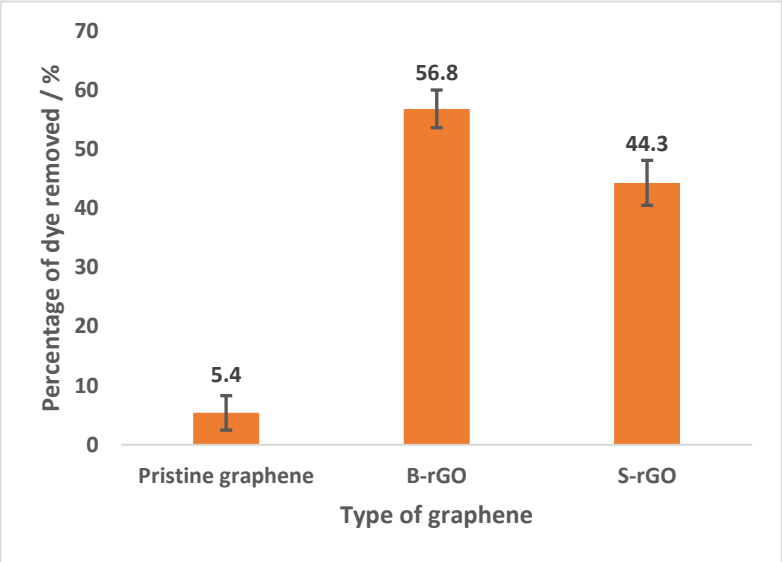

Figure 5: Effect of heteroatom doping on removal of direct red dye

Taking into account that the adsorption of direct red dye molecules on graphene aids the degradation of direct red dye, the effect of heteroatom doping on the adsorption of direct red dye was investigated in the absence of PMS. Based on figure 5, B-rGO and S-rGO outperformed pristine graphene in the adsorption of direct red dye by close to 8 times. B-rGO also outperformed S-rGO, with the Mann Whitney U-Test yielding a value of 0.0357 (<0.05)

By incorporating sulfur atoms into the graphene structure, the number of electrons in the carbon structure increases, leading to an increase in electron cloud density. This in turn causes stronger π-π interactions to be formed between the graphene structure and direct red dye, leading to more direct red dye molecules being adsorbed. By incorporating boron atoms in the graphene structure, it is postulated that the difference in electronegativity between boron (2.04) and carbon atoms (2.55) leads to a charge separation and differing electron density in the carbon structure (Yu et al., 2018). This leads to stronger π-π interactions to be formed between the B-rGO structure and direct red molecule, causing more direct red dye to be

adsorbed. However, the effect is lesser when compared to the increased electron cloud in S-rGO, as a larger electron cloud would play a larger role in the strength of π-π interactions.

3.4 Effect of heteroatom doping on degradation of direct red dye

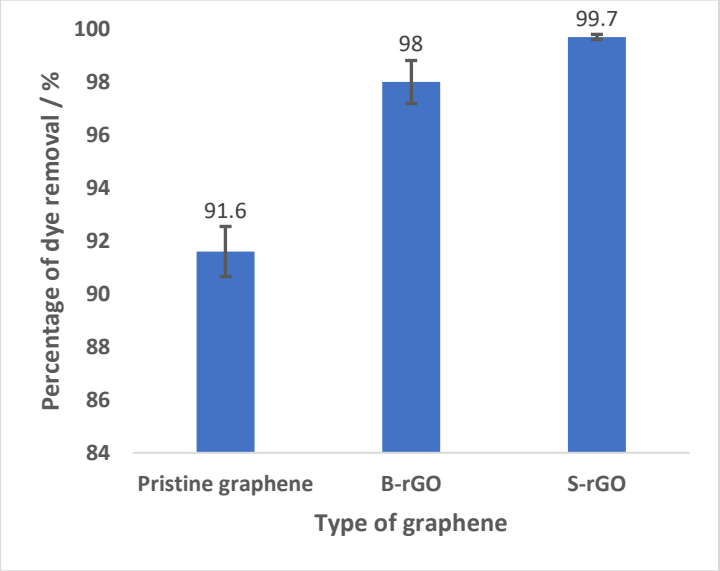

Figure 6: Effect of heteroatom doping on degradation of direct red dye

Figure 6 shows that B-rGO and S-rGO outperformed pristine graphene in the degradation of direct red dye. B-rGO and S-rGO are equally effective in the degradation of direct red dye, with a Mann Whitney U-test yielding a value of 0.0111 (>0.05).

The difference between heteroatom doped rGO and pristine graphene could firstly be caused by the increased adsorption capabilities for both B-rGO and S-rGO caused by heteroatom doping, thereby aiding in the degradation efficiency of heteroatom-doped rGO.

The aforementioned difference could also be due to the increase in defective sites in B-rGO and S-rGO caused by the doping of boron and sulfur respectively, compared to the number of defective sites in pristine graphene. As a result, B-rGO and S-rGO have more active sites for the oxidation of PMS, leading to an increase in generation of highly reactive radical species for the degradation of both organic dyes.

3.5 Generation of hydroxyl radicals using heteroatom-doped rGO

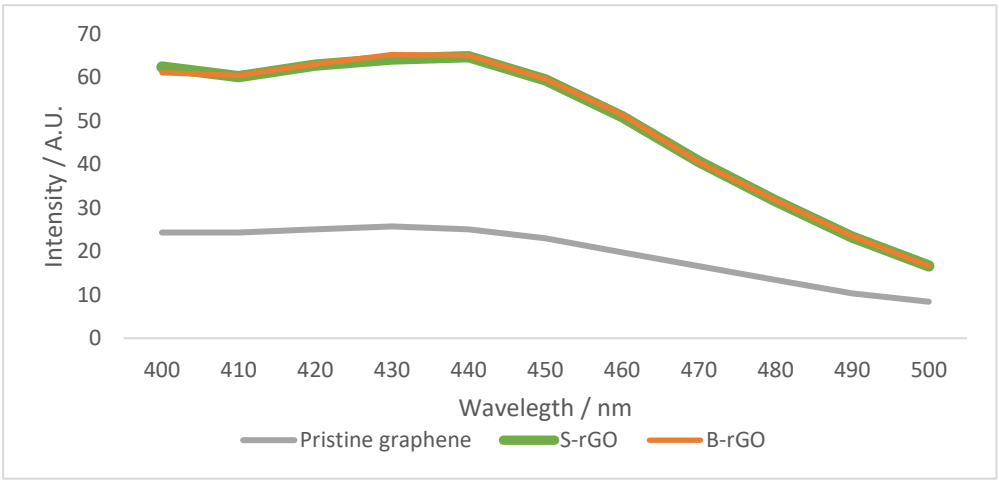

Figure 7: Photoluminescence spectra for both heteroatom-doped graphene and pristine graphene

Figure 7 shows the photoluminescence spectra obtained from the qualitative analysis of hydroxyl radicals using terephthalic acid (TA). The individual graphs can be found in appendix B. A peak at around 439nm is visible for both heteroatom-doped rGO and pristine graphene that reacted with PMS was visible, which implies the presence of hydroxyl radicals in the solution. The intensity of the peak at 439nm can be used to quantitatively determine the difference in the amount of hydroxyl radicals generated from both heteroatom-doped graphene and pristine graphene. Peaks of higher intensity were obtained when graphene underwent heteroatom doping, suggesting that the amount of OH• generated increased when heteroatoms such as sulfur and boron were induced into the graphene structure due to an increase in activation of PMS. Peaks of similar intensity were obtained for both S-rGO and B-rGO, suggesting that both sulfur and boron doping are able to increase the amount of OH• through the increased activation of PMS. This could explain the insignificant difference in percentage of direct red degraded between S-rGO and B-rGO.

4 Conclusion and Future Work

Sulfur and boron atoms were successfully incorporated into the single layer graphene structure, with the morphology of B-rGO being rough and uneven. Both S-rGO and B-rGO were effective in the activation of PMS; both could remove close to 100% of the tested direct red dye. Both B-rGO and S-rGO outperformed pristine graphene in the adsorption of direct red dye by, as well as in the degradation of direct red dye. B-rGO outperformed S-rGO in the adsorption of direct red dye but both were equally effective in the degradation of direct red dye. More OH• was generated when graphene was heteroatom-doped, thus further substantiating that heteroatom doping increases the activation of PMS and increases the degradation of direct red dye. Heteroatom doping of graphene is an effective method in increasing the activation of PMS and enhancing the removal of organic red dyes by PMS.

In the future, the reusability of S-rGO and B-rGO in the degradation of direct red dye in the presence of PMS can be investigated. High Performance Liquid Chromatography-Mass spectrometry can also be used to determine the degradation pathway of direct red dye.

For application purposes, heteroatom-doped rGO and PMS can be incorporated into a membrane filter and used in a filter bottle (Appendix D, page 17), which also includes a sand layer for the removal of solid particles and algae, and a spent tea waste membrane filter at the bottom to quench any radicals present in the filtrate. Such a filter bottle could be used in low-income families where access to clean drinking water is not easily accessible.

References

Beg, K. R., & Ali, S. (2008). Chemical contaminants and toxicity of Ganga River sediment from up and down stream area at Kanpur. *American Journal of Environmental Sciences*, 4(4)

Devi, P., Das, U. & Dalai, A.K. (2016). In-situ chemical oxidation: Principle and applications of peroxide and PS treatments in wastewater systems. *Science Total Environment*, 571, 643-657.

Duan, X., Indrawirawan, S., Sun, H. & Wang, S. (n.d.) Effects of nitrogen-, boron-, and phosphorus- doping or cooping on metal-free graphene catalysis. Retrieved from https://espace.curtin.edu.au/bitstream/handle/20.500.11937/30067/227706.pdf?sequence=2

Duan, X., Sun, H., Ao, Z., Li, Z., Wang, G. & Wang, S. (2016). Unveiling the active sites of graphene-catalyzed peroxymonosulfate activation. *Carbon*, 107, 371-378. Retrieved from https://iehpc.gdut.edu.cn/2016-32.pdf

Karikalan, N., Karthik, R., Chen, S.M., Karuppiah, C. & Elangovan, A. (2017). Sonochemical Synthesis of Sulfur Doped Reduced Graphene Oxide Supported CuS Nanoparticles for the Non-Enzymatic Glucose Application. *Scientific Reports*, 2494. Retrieved from https://www.nature.com/articles/s41598-017-02479-5#Fig2

Mayor, S. (2017). Pollution is linked to one in six deaths worldwide, study estimates. *Bmj*. doi:10.1136/bmj.j4844

Mia, R., Selim, M., Shamim, A.M., Chowdhury, M., Sultana, S., Armin, M., Hossain, M., Akter, R., Dey, S. & Naznin, H. (2019). Review on various types of pollution problem in textile dyeing & printing industries of Bangladesh and recommendation for mitigation. *Journal of Textile Engineering & Fashion Technology*, 5(4), 220-226. Retrieved from https://medcraveonline.com/JTEFT/JTEFT-05-00205.pdf

Novotny, C., Dias, N., Kapanen, A., Malachova, K., Vandrovcova, M., M.Itavarra, Lima, N. (2006). Comarative use of bacterial, algal and protozoan tests to study toxicity of azo and anthraquinone dyes. *Chemosphere*, 63

Wang, J. & Wang, S. (2018). Activation of persulfate (PS) and peroxymonosulfate (PMS) and application for the degradation of emerging contaminants. *Chemical Engineering Journal*, 334, 1502-1517.

Yu, X., Han, P., Wei, Z., Huang, L., Gu, Z., Peng, S., Ma, J. & Zheng, G. (2018). Boron-Doped Graphene for Electrocatalytic N_2 Reduction. *Joule*, 2(8), 1602-1622. Retrieved from https://www.sciencedirect.com/science/article/pii/S2542435118302435#!

Appendix A: Calibration curve for direct red dye

A calibration curve was obtained for direct red dye. As the coefficient of determination (R^2) obtained for the linear equation derived is close to 1, it can be used with very high accuracy to determine the concentration of direct red from the absorbance obtained from UV-Vis spectrophotometer, for all subsequent dye degradation studies.

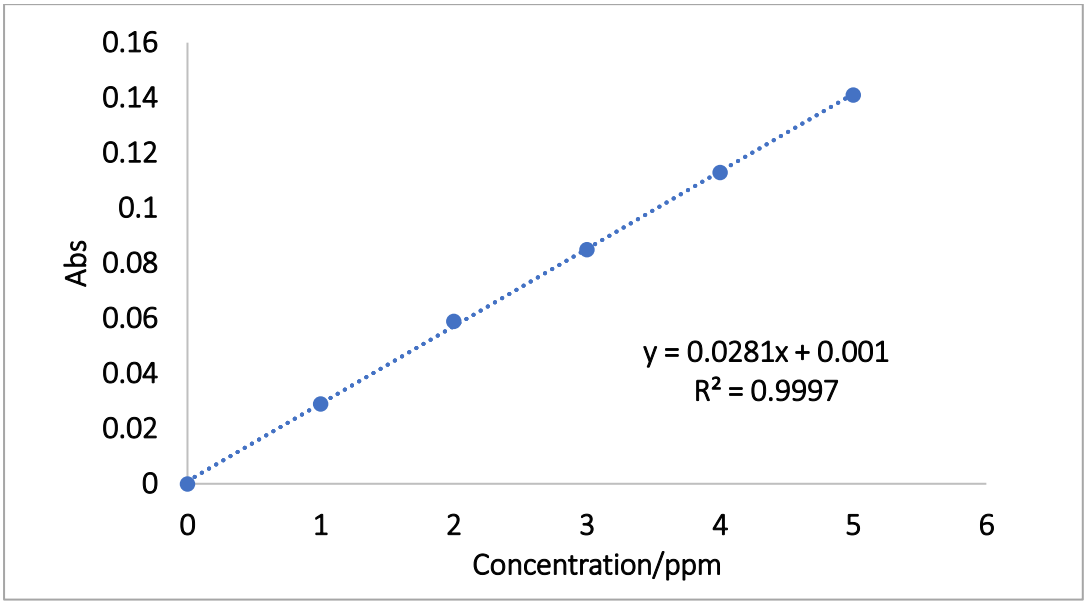

Figure 8: Calibration curve for direct red dye

Appendix B: Quantification of hydroxyl radicals

Terephthalic acid (TA) is a well-known OH• scavenger which does not react with any other radical species, such as O_2^-, HO_2 and H_2O_2. As shown in figure 9, OH• can covert TA to 2-hydroxyterephthalic acid (HTA), which can be detected by fluorescence measurement. When the solution containing TA and HTA is irradiated by UV light (λ=310nm), HTA can emit light at λ=439nm, while TA molecules do not. The relative intensity (a.u.) of the peak at λ=439nm would represent the relative concentration of HTA, and consequently the relative concentration of OH•, in the solution.

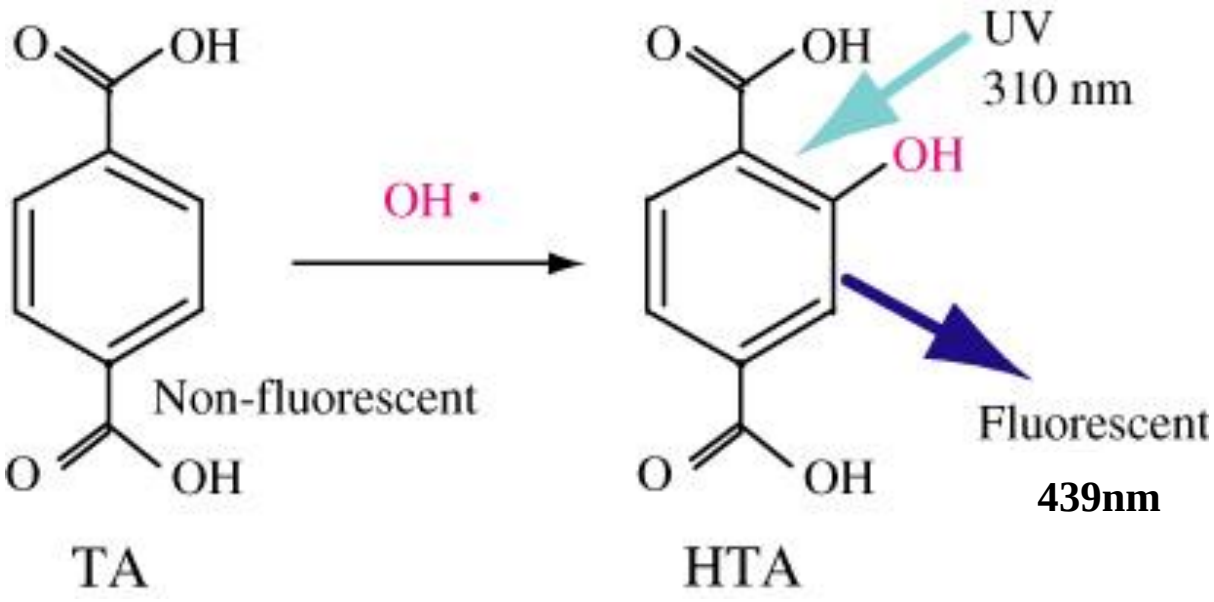

Figure 9: Conversion of TA to HTA in the presence of OH•

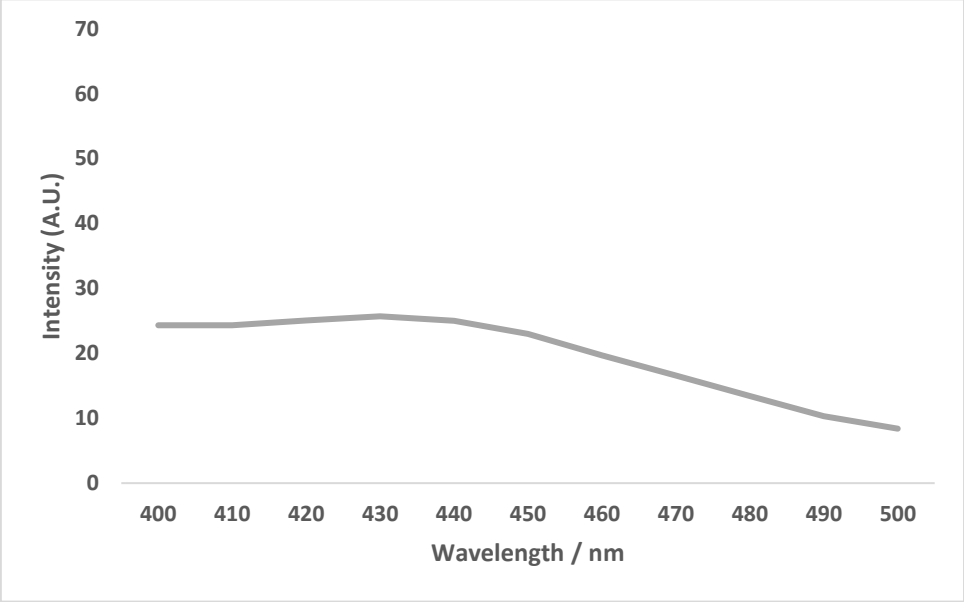

Figure 10: Photoluminescence spectra for pristine graphene

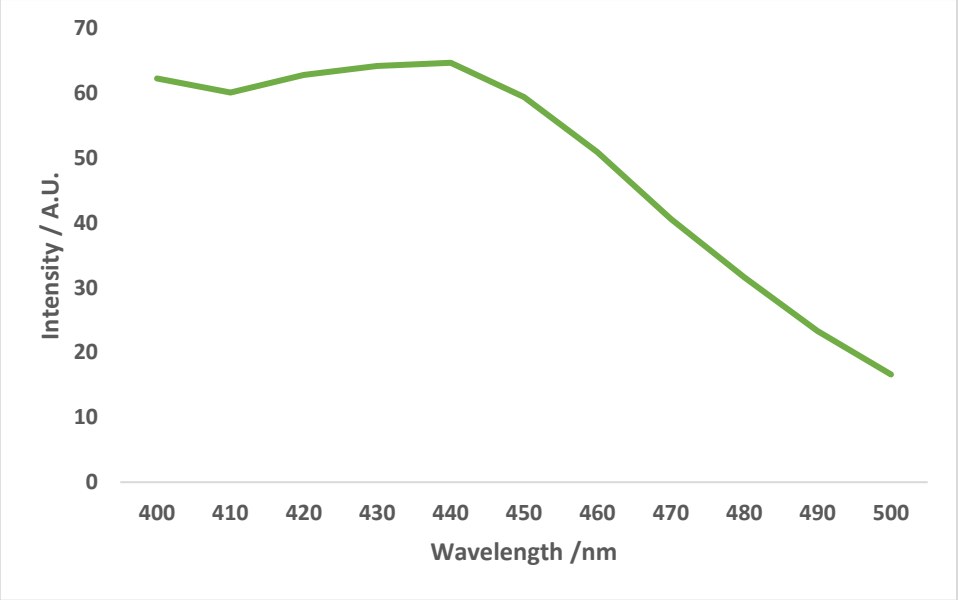

Figure 11: Photoluminescence spectra for S-rGO

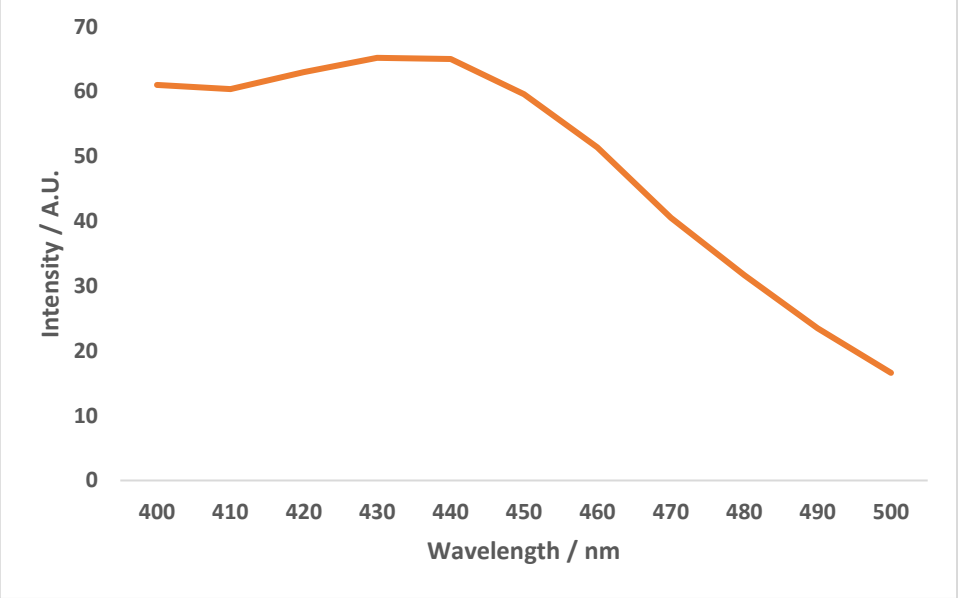

Figure 12: Photoluminescence spectra for B-rGO

As seen in Figure 10, Figure 11 and Figure 12, a peak at λ=439nm was detected, indicating a presence of OH• in all 3 samples. However, the intensity of the peak for pristine graphene is close to half of the intensity of the peak both B-rGO and S-rGO, indicating that a lower concentration of OH• was produced by pristine graphene than B-rGO and S-rGO and suggests that lesser PMS was activated by pristine graphene. On the other hand, the relative

intensities of the peak at λ=439nm for both B-rGO and S-rGO were close, indicating that the concentration of OH• produced for both B-rGO and S-rGO were close and suggests that the amount of PMS activated by both rGOs are close, which explains why they were equally effective in the degradation of direct red dye.

Appendix C: Fourier Transform Infrared (FTIR) Spectrum for pristine graphene

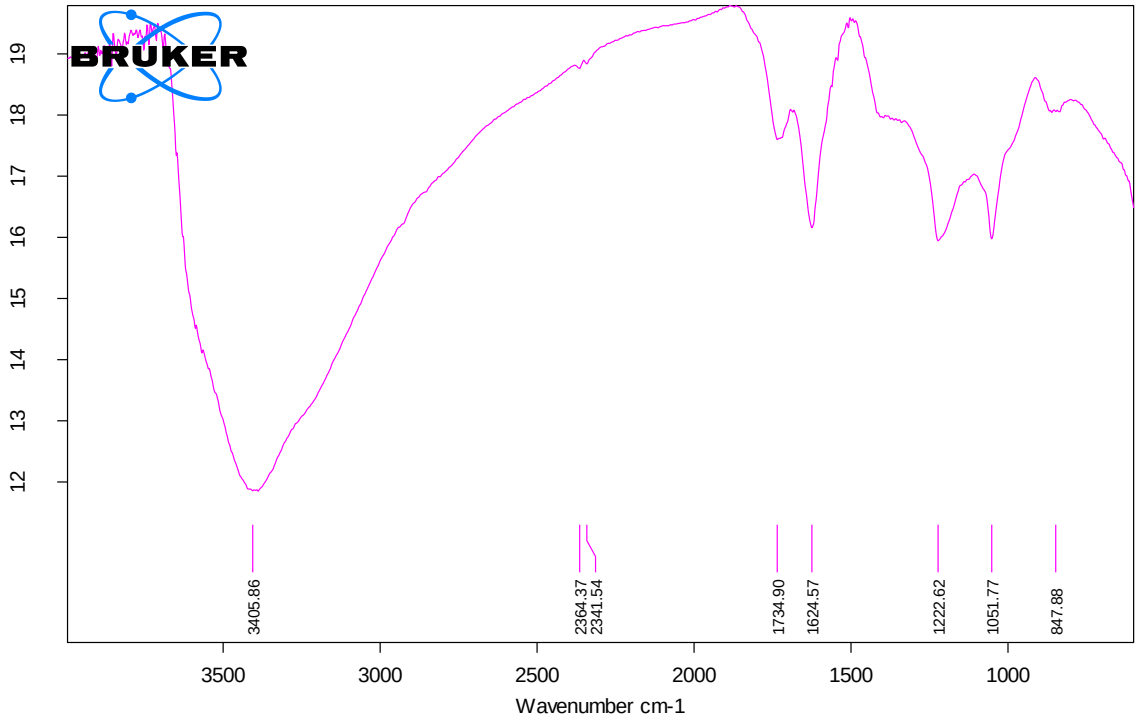

Figure 13: Conversion of TA to HTA in the presence of OH•

Figure 13 shows the FTIR spectrum for pristine graphene. O-H stretching (3406cm^{-1}), C=O stretching (1735cm^{-1}), C=C stretching (1625 cm^{-1}), C-OH stretching vibration (1223cm^{-1}) and C-O stretching mode (1050cm^{-1}), which are characteristics of pristine graphene.

Appendix D: Heteroatom doped rGO filter bottle

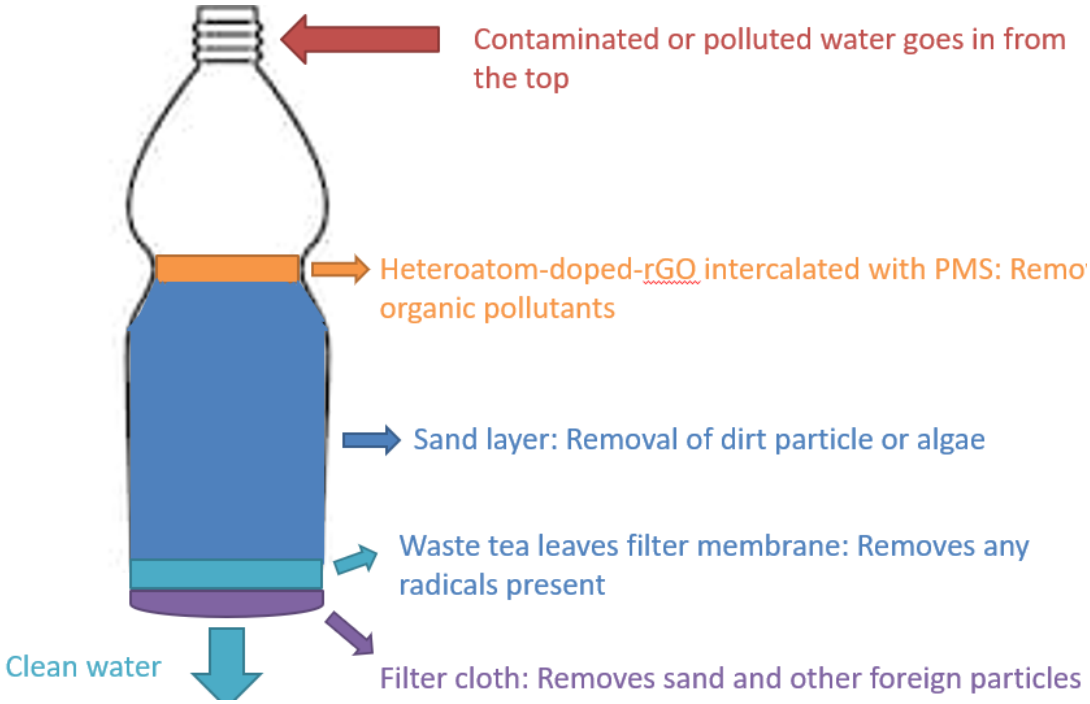

Figure 14: Example of heteroatom doped rGO filter bottle

Figure 14 shows a potential heteroatom doped rGO filter bottle which can be used for quick purification of wastewater contaminated with organic pollutants such as dyes in impoverished areas where access to clean drinking waters is limited.

The first layer would be the filter membrane, which contains the heteroatom doped rGO intercalated with PMS. At this layer, the dyes would be adsorbed and broken down by the OH• and SO_4^{-}• produced from the activation of PMS.

The second layer would be the sand layer, which is to slow down the movement of water to provide ample time for the adsorption and degradation of the dye. The sand layer would also help to remove any dirt particles or algae present in the contaminated waters.

The third layer would be the waste tea leaves filter membrane, which is able to quench and remove any radicals present to ensure that the filtrate is safe for consumption.

The final layer would be the filter cloth, which would remove the sand any other foreign particles, with the filtrate being safe and clean drinking water that is free from any organic pollutants such as dyes.